On the Performance of SPAD-Based Optical Wireless Communication with ACO-OFDM

Shenjie Huang, Cheng Chen, Mohammad Dehghani Soltani, Robert Henderson, Harald Haas, and Majid Safari

***Abstract*—The nonlinear distortion introduced by the dead time strongly limits the throughput of the highly sensitive SPAD-based optical wireless communication (OWC) systems. Optical OFDM can be employed in the systems with SPAD arrays to improve the spectral efficiency. In this work, a theoretical performance analysis of SPAD-based OWC system with asymmetrically-clipped optical OFDM (ACO-OFDM) is presented. The impact of the SPAD nonlinearity on the system performance is investigated. In addition, the comparison of the considered scheme with DCO-OFDM is presented showing the distinct reliable operation regimes of the two schemes. In low optical power regimes, ACO-OFDM outperforms DCO-OFDM with around 4 dB power gain achieved by 16-QAM ACO-OFDM over 4-QAM DCO-OFDM. However, DCO-OFDM is in turn more preferable in high power regimes which extends the maximal tolerable received optical power by 7.4 dB.**

***Index Terms*—Optical wireless communication, orthogonal frequency division multiplexing, single-photon avalanche diode.**

I. Introduction

In recent decades, the optical wireless communication (OWC) has been continuously gaining interest in both industry and academia and is considered as a potential candidates to provide more powerful wireless connections in the future. The performance of OWC can be strongly degraded by the occasional outages introduced by multiple effects such as adverse weather condition and user mobility in outdoor and indoor scenarios, respectively. One effective way of improving the performance of OWC systems under weak power reception is employing highly sensitive photon counting receivers such as a single-photon avalanche diode (SPAD). A SPAD receiver is achieved by biasing a traditional linear photodiode above the breakdown voltage so that it operates in the 'Geiger mode' [1]. When a photon is received by SPAD receivers, an avalanche is triggered generating a striking electrical output pulse which realizes the single photon detection.

Although a SPAD receiver has photon count capability, after each avalanche it has to be quenched for a short period of time when it becomes blind to any incident photon arrivals, which is also know as the *dead time*. The throughputs of the OWC systems with SPAD receivers are strongly limited by the nonlinearity induced by the dead time [1]. Although most of the prior SPAD-based OWC works focus on the on-off keying (OOK) [2], some works have been conducted to investigate the application of optical orthogonal frequency division multiplexing (OFDM) in SPAD-based OWC systems to improve the spectral efficiency [3], [4]. In particular, in [3] a record data rate of 5 Gbps is achieved experimentally using a commercial SPAD receiver with the employment of the optical OFDM and nonlinear equalizer. Despite the aforementioned experimental works, a theoretical performance analysis of SPAD-based OWC systems with direct-current-biased optical OFDM (DCO-OFDM) was conducted very recently [5]. Besides DCO-OFDM, asymmetrically-clipped optical OFDM (ACO-OFDM) is another commonly used optical OFDM scheme which does not require a DC bias and enjoys a better power efficiency [6]. It is concluded that ACO-OFDM is well suited to some practical applications such as the visible light communication (VLC) with dimming control. However, to the best of our knowledge, the theoretical signal-to-noise ratio (SNR) and error performance analysis of SPAD-based OWC systems with ACO-OFDM in the presence of practical issues such as signal clipping, signal-dependent shot noise, and SPAD dead time is still missing. In this work, we aim to fill this research gap and derive the analytical expressions of the SNR and bit error rate (BER) of the considered system. In addition, the influence of the unique SPAD nonlinearity on the system performance is investigated and an in-depth comparison with SPAD DCO-OFDM is presented.

This work was supported by Engineering and Physical Sciences Research Council (EPSRC) under Grant EP/S016570/1 (TOWS). (Corresponding author: Shenjie Huang.)

S. Huang, M. D. Soltani, R. Henderson, and M. Safari are with the School of Engineering, the University of Edinburgh, Edinburgh EH9 3JL, UK. C. Chen and H. Haas are with LiFi Research and Development Centre, University of Strathclyde, Glasgow G1 1RD, UK. (e-mail: shenjie.huang@ed.ac.uk; c.chen@strath.ac.uk; m.dehghani@ed.ac.uk; robert.henderson@ed.ac.uk; harald.haas@strath.ac.uk; majid.safari@ed.ac.uk).

II. SPAD-Based ACO-OFDM System

A. ACO-OFDM Transmission

For a SPAD-based OWC system with ACO-OFDM, at the transmitter, the input bit stream is transformed into a complex symbol stream by the M-quadrature amplitude modulation (QAM) modulator, where M denotes the constellation size. The symbol stream is then serial-to-parallel (S/P) converted to form vectors suitable for inverse fast Fourier transform (IFFT) operation. Considering a K-point fast Fourier transform (FFT) operation, only the odd subcarriers of the first half of the OFDM frame with index $k = 1, 3, 5, \cdots, K/2-1$ are used to carry the information, whereas the even subcarriers are left unused. Therefore, the number of information carrying subcarriers is $K' = K/4$. Hermitian symmetry is applied to the rest of the OFDM frame in order to obtain the real-valued symbols after the IFFT operation. Denote the generated OFDM frame as $X[k]$, the time-domain signal $x[n]$ can be obtained after the IFFT as $x[n] = \frac{1}{\sqrt{K}}\left(\sum_{k=0}^{K-1} X[k] e^{\frac{2\pi nkj}{K}}\right)$. For systems with relatively large number of subcarriers, i.e., $K > 64$, $x[n]$ can be approximated as a set of independent identical distributed random variables with zero-mean Gaussian distribution according to the central limit theorem (CLT) [7]. Considering the uniform power allocation over

This is a peer reviewed, accepted author manuiscript of the following research aritcle: Huang, S., Chen, C., Soltani, M. D., Henderson, R., Haas, H., & Safari, M. (2023). On the performance of SPAD-based optical wireless communication with ACO-OFDM. *IEEE Communications Letters.* https://doi.org/10.1109/lcomm.2023.3271617

the subcarriers, the variance of signal should be $\sigma_X^2 = 2$ to ensure that $x[n]$ is with unit variance [8]. Since only the odd subcarriers are utilized, the time-domain signal $x[n]$ has the following anti-symmetry [7]

$$x[n] = -x\left[n + K/2\right] \quad \text{for} \quad n \in [0, K/2-1]\,. \tag{1}$$

Therefore, the clipping of all negative samples at the transmitter does not introduce any information loss and the information can still be successfully decoded at the receiver [8]. Considering that the peak-to-average power ratio (PAPR) of the generated signal $x[n]$ is relatively high whereas practical light sources are with limited dynamic ranges, $x[n]$ should also be properly clipped at a top clipping level κ. Hence, the clipped signal can be expressed as

$$x_{\rm c}[n] = \begin{cases} \kappa, & \text{if} \quad x[n] \geq \kappa, \\ x[n], & \text{if} \quad 0 < x[n] < \kappa, \\ 0, & \text{if} \quad x[n] \leq 0. \end{cases} \tag{2}$$

After applying scaling and digital-to-analog conversion, the resultant electrical signal is used to drive the light source. In effect, the optical power of the nth time-domain OFDM sample emitted from the source is given by $x_{\rm t}[n] = \xi\, x_{\rm c}[n]$ where ξ denotes the scaling factor. Denoting the maximal optical power of the light source as $P_{\max}$, $\xi\kappa = P_{\max}$ should be satisfied, which leads to $\xi = P_{\max}/\kappa$. The average transmit optical power is given by $\overline{P}_{\rm Tx} = \xi\left[1/\sqrt{2\pi} - f_N(\kappa) + \kappa\, Q(\kappa)\right]$, where $f_N(x)$ is the probability density function (PDF) of a standard Gaussian distribution and $Q(\cdot)$ denotes the Q-function. The block diagram of the SPAD-based OWC system with ACO-OFDM is similar to that with DCO-OFDM presented in Fig. 1 of [5], whereas the addition of DC bias is not required. Note that in this work the lower limit of the light source dynamic range is assumed to be zero which leads to the additional DC biasing unnecessary [6]. However, the biasing of $x_{\rm t}[n]$ is required for cases with non-zero lower limit [9].

B. SPAD Receivers

The photodetection process of an ideal photon counter can be modelled using Poisson statistics. However, the performance of the practical SPAD-based receivers suffer from the non-ideal effects such as dead time, photon detection efficiency (PDE), dark count rate (DCR), afterpulsing and crosstalk. To mitigate the significant nonlinearity effects introduced by the dead time and improve the photon counting capability, arrays of SPADs are commonly used in OWC [1], [2]. Considering that the channel loss is ζ, the average received signal optical power is given by $\overline{P}_{\rm Rx} = \zeta\, \overline{P}_{\rm Tx}$. Assuming a precise time synchronization between transceivers, the received optical power when the nth OFDM sample is transmitted can be expressed as $P_{\rm Rx}[n] = \zeta x_{\rm t}[n]$. The corresponding incident photon rate of the SPAD array is $\lambda_{\rm a}[n] = \mathcal{C}_{\rm s} x_{\rm t}[n] + \mathcal{C}_{\rm n}$ where

$$\begin{cases} \mathcal{C}_{\rm s} = \Upsilon_{\rm PDE}\zeta\left(1 + \varphi_{\rm AP} + \varphi_{\rm CT}\right)/E_{\rm ph}, \\ \mathcal{C}_{\rm n} = \left(\vartheta_{\rm DCR} + \vartheta_{\rm B}\right)\left(1 + \varphi_{\rm AP} + \varphi_{\rm CT}\right), \end{cases} \tag{3}$$

$\Upsilon_{\rm PDE}$ is the PDE of the SPAD, $E_{\rm ph}$ is the photon energy, $\vartheta_{\rm B}$ denotes the background photon rate, and $\vartheta_{\rm DCR}$, $\varphi_{\rm AP}$ and $\varphi_{\rm CT}$ refer to the DCR of the array, the probabilities of afterpulsing and crosstalk, respectively. The photon rate $\vartheta_{\rm B}$ equals to $\Upsilon_{\rm PDE}P_{\rm B}/E_{\rm ph}$ where $P_{\rm B}$ is the ambient light power.

In this work, we employ passive quenched (PQ) based SPAD receiver which is commonly used in the commercial products. The SPAD array detector outputs the detected photon count during every OFDM sample duration $T_{\rm s}$. Denote that, after the S/P mapping, the detected photon count of the SPAD array when the nth OFDM sample is transmitted as $y[n]$. When the array size is relatively large (more than several hundreds), according to the CLT, $y[n]$ is approximately Gaussian distributed with mean and variance given by [1]

$$\mu_{\rm a}(x[n]) = \lambda_{\rm a}[n] T_{\rm s} \exp\left(-\lambda_{\rm a}[n]\tau_{\rm d}/N_{\rm a}\right), \tag{4}$$

and

$$\sigma_{\rm a}^2(x[n]) = \mu_{\rm a}(x[n]) - \frac{\lambda_{\rm a}^2[n] T_{\rm s}\tau_{\rm d}}{N_{\rm a}} \exp\left(-\frac{2\lambda_{\rm a}[n]\tau_{\rm d}}{N_{\rm a}}\right)\left(2 - \frac{\tau_{\rm d}}{T_{\rm s}}\right), \tag{5}$$

respectively, where $N_{\rm a}$ denotes the number of SPADs in the array and $\tau_{\rm d}$ refers to the dead time. Note that (4) indicates that with the increase of the incident photon rate $\lambda_{\rm a}[n]$, the detected photon count firstly increases and then decreases, hence the received optical signal is nonlinearly distorted by the SPAD receiver. The detected photon count $y[n]$ can be written by

$$y[n] = \mu_{\rm a}(x[n]) + w_{\rm s}[n], \tag{6}$$

where $w_{\rm s}[n]$ represents the shot noise which is Gaussian distributed with zero mean and signal dependent variance given by (5). At the receiver, the signal $y[n]$ is then converted back to the frequency-domain using the FFT operation given by $Y[k] = \frac{1}{\sqrt{K}}\left(\sum_{n=0}^{K-1} y[n] e^{-\frac{2\pi n k j}{K}}\right)$. Finally, after the single-tap equalization, P/S mapping, and QAM demodulation, the recovered bit steam can be achieved.

III. Theoretical Analysis of SPAD ACO-OFDM

In this section, we aim to derive the closed-form expressions of the SNR of SPAD ACO-OFDM based on which the BER can be further calculated. Two nonlinear distortions exist in the considered system. The first is the clipping-induced distortion as presented in (2), which also exists in standard OFDM-based OWC systems with linear receivers [8]. The second is the additional unique SPAD-induced distortion given in (4). We combine these two nonlinear distortions and investigate the system performance in the presence of the effective nonlinear distortion. By substituting (2) into (4), the combined nonlinear distortion of the transmitted signal $x[n]$ is given by

$$\mu_{\rm a}(x[n]) = \tag{7}$$
$$\begin{cases} \left(\psi_1\kappa + \mathcal{C}_{\rm n}\right) T_{\rm s} \exp\left[-\frac{(\psi_1\kappa + \mathcal{C}_{\rm n})\tau_{\rm d}}{N_{\rm a}}\right], & \text{if } x[n] \geq \kappa, \\ \left(\psi_1 x[n] + \mathcal{C}_{\rm n}\right) T_{\rm s} \exp\left[-\frac{(\psi_1 x[n] + \mathcal{C}_{\rm n})\tau_{\rm d}}{N_{\rm a}}\right], & \text{if } 0 < x[n] < \kappa, \\ \mathcal{C}_{\rm n} T_{\rm s} \exp\left(-\frac{\mathcal{C}_{\rm n}\tau_{\rm d}}{N_{\rm a}}\right), & \text{if } x[n] \leq 0. \end{cases}$$

where $\psi_1 = \mathcal{C}_{\rm s} P_{\max}/\kappa$. According to the Bussgang theorem, the nonlinear distortion in an OFDM-based system can be described by a gain factor (α) and an additional signal-independent distortion-induced noise ($w_{\rm d}[n]$) [7], [8] as

$$\mu_{\rm a}(x[n]) = \alpha x[n] + w_{\rm d}[n]. \tag{8}$$

The gain factor α can be calculated as [5]

$$\alpha = \frac{\psi_1^2 \tau_{\rm d} T_{\rm s}}{\sqrt{2\pi} N_{\rm a}} \left\{ \exp\left[-\frac{\kappa^2}{2} - \frac{\tau_{\rm d}}{N_{\rm a}} \left(\psi_1 \kappa + \mathcal{C}_{\rm n} \right) \right] - e^{-\frac{\tau_{\rm d} \mathcal{C}_{\rm n}}{N_{\rm a}}} \right\} + \psi_1 \, T_{\rm s} \, e^{-\frac{\mathcal{C}_{\rm n} \tau_{\rm d}}{N_{\rm a}} + \frac{\psi_1^2 \tau_{\rm d}^2}{2 N_{\rm a}^2}} \left[1 + \frac{\psi_1^2 \tau_{\rm d}^2}{N_{\rm a}^2} - \frac{\mathcal{C}_{\rm n} \tau_{\rm d}}{N_{\rm a}} \right] \times \left[Q\left(\frac{\psi_1 \tau_{\rm d}}{N_{\rm a}} \right) - Q\left(\kappa + \frac{\psi_1 \tau_{\rm d}}{N_{\rm a}} \right) \right], \quad (9)$$

which describes the scaling of the undistorted signal after passing through the effective additive noise channel introduced by the nonlinear distortion and can be used to measure the received signal power. The variance of $w_{\rm d}[n]$, denoted as $\sigma^2_{w_{\rm d}}$, is given by

$$\sigma^2_{w_{\rm d}} = \mathbb{E}\left\{ \mu^2_{\rm a}(x[n]) \right\} - \mathbb{E}^2 \left\{ \mu_{\rm a}(x[n]) \right\} - \alpha^2, \quad (10)$$

where $\mathbb{E}\{\cdot\}$ denotes the statistical expectation. The two moments of $\mu_{\rm a}(x[n])$ in (10) can be found in [5].

By plugging (8) into (6), the SPAD output $y[n]$ can be rewritten as $y[n] = \alpha x[n] + w_{\rm d}[n] + w_{\rm s}[n]$. After applying FFT operation, the signal in the frequency domain can be expressed as

$$Y[k] = \alpha X[k] + W_{\rm d}[k] + W_{\rm s}[k], \quad (11)$$

where $W_{\rm d}[k]$ and $W_{\rm s}[k]$ denote the FFT of $w_{\rm d}[n]$ and $w_{\rm s}[n]$, respectively. When the number of subcarriers is sufficiently large, CLT applies and both $W_{\rm d}[k]$ and $W_{\rm s}[k]$ are zero-mean Gaussian noise terms [7]. As a result, in the frequency domain the received signal is the transmitted signal multiplied by a gain factor plus two additive Gaussian noises. Therefore, in order to achieve the closed-form SNR, the analytical expressions of both $W_{\rm d}[k]$ and $W_{\rm s}[k]$ should be derived. The variance of the shot noise $W_{\rm s}[k]$ for the considered system with ACO-OFDM, denoted as $\sigma^2_{W_{\rm s}}$, is identical to that with DCO-OFDM which has been derived in our previous work [5]. Note that as proved in Proposition 4 of [5], $\sigma^2_{W_{\rm s}}$ equals to the average of the signal dependent shot noise variance in the time domain and hence is signal independent.

Now let's derive the variance of the distortion-induced noise in the frequency domain $W_{\rm d}[k]$. The variance of $W_{\rm d}[k]$ can be calculated as (12) at the top of the next page where $n_{\rm f}$ denotes the anti-symmetrical index of n as

$$n_{\rm f} = \begin{cases} n + \frac{K}{2} & \text{if} \quad n \leq \frac{K}{2} - 1, \\ n - \frac{K}{2} & \text{if} \quad n > \frac{K}{2} - 1. \end{cases} \quad (13)$$

Note that due to the anti-symmetry property of the time-domain ACO-OFDM samples shown in (1), $w_{\rm d}[n]$ and $w_{\rm d}[n_{\rm f}]$ are correlated. In fact, because of the existence of this correlation, $\sigma^2_{W_{\rm d}}[k]$ does not simply equal to $\sigma^2_{w_{\rm d}}$, which differs from the system with DCO-OFDM [5]. The term $\mathcal{T}_1$ in (12) can be calculated as $\mathcal{T}_1 = \sum_{n=0}^{\frac{K}{2}-1} e^{\pi k j} + \sum_{n=\frac{K}{2}}^{K-1} e^{-\pi k j} = K \cos(\pi k)$. On the other hand, for $k \geq 1$ the term $\mathcal{T}_2$ in (12) can be calculated as

$$\mathcal{T}_2 = -\sum_{n=0}^{K-1} e^{-\frac{2\pi n k j}{K}} \left(e^{\frac{2\pi n k j}{K}} + e^{\frac{2\pi n_{\rm f} k j}{K}} \right) = -K - \sum_{n=0}^{K-1} e^{-\frac{2\pi (n - n_{\rm f}) k j}{K}} = -K - \sum_{n=0}^{\frac{K}{2}-1} e^{\pi k j} - \sum_{n=\frac{K}{2}}^{K-1} e^{-\pi k j} = -K - K\cos(\pi k). \quad (14)$$

Both $\mathcal{T}_1$ and $\mathcal{T}_2$ are distinct for odd and even subcarriers, hence the distortion-induced noise variances are different for these subcarriers. For information carrying odd k, one can get $\mathcal{T}_1 = -K$ and $\mathcal{T}_2 = 0$. Therefore, the variance of the distortion-induced noise in the frequency domain can be expressed as

$$\sigma^2_{W_{\rm d}} = \sigma^2_{w_{\rm d}} + \mathbb{E}^2\{w_{\rm d}[n]\} - \mathbb{E}\{w_{\rm d}[n] w_{\rm d}[n_{\rm f}]\}. \quad (15)$$

Invoking the definition of $w_{\rm d}[n]$ in (8), one has $\mathbb{E}\{w_{\rm d}[n]\} = \mathbb{E}\{\mu_{\rm a}(x[n])\}$. Substituting (10) into (15) results in

$$\sigma^2_{W_{\rm d}} = \mathbb{E}\left\{ \mu^2_{\rm a}(x[n]) \right\} - \alpha^2 - \mathbb{E}\{w_{\rm d}[n] w_{\rm d}[n_{\rm f}]\}. \quad (16)$$

The moment $\mathbb{E}\left\{ \mu^2_{\rm a}(x[n]) \right\}$ can be found in [5]. For the correlation term $\mathbb{E}\{w_{\rm d}[n] w_{\rm d}[n_{\rm f}]\}$, one can get

$$\mathbb{E}\{w_{\rm d}[n] w_{\rm d}[n_{\rm f}]\} = \mathbb{E}\left\{ \mu_{\rm a}(x[n]) \mu_{\rm a}(x[n_{\rm f}]) \right\} - \alpha \mathbb{E}\left\{ \mu_{\rm a}(x[n]) x[n_{\rm f}] \right\} - \alpha \mathbb{E}\left\{ \mu_{\rm a}(x[n_{\rm f}]) x[n] \right\} + \alpha^2 \mathbb{E}\left\{ x[n] x[n_{\rm f}] \right\}. \quad (17)$$

From (1) and (13), the equation $x[n_{\rm f}] = -x[n]$ holds and substituting this into (17) leads to

$$\mathbb{E}\{w_{\rm d}[n] w_{\rm d}[n_{\rm f}]\} = \mathbb{E}\left\{ \mu_{\rm a}(x) \mu_{\rm a}(-x) \right\} + \alpha \mathbb{E}\left\{ \mu_{\rm a}(x) x \right\} - \alpha \mathbb{E}\left\{ \mu_{\rm a}(-x) x \right\} - \alpha^2, \quad (18)$$

where the sample index n is dropped for simplicity. Since the term $\mathbb{E}\left\{ \mu_{\rm a}(x) x \right\}$ and $\mathbb{E}\left\{ \mu_{\rm a}(-x) x \right\}$ equals to α and $-\alpha$, respectively, expression (18) can be rewritten as

$$\mathbb{E}\{w_{\rm d}[n] w_{\rm d}[n_{\rm f}]\} = \mathbb{E}\left\{ \mu_{\rm a}(x) \mu_{\rm a}(-x) \right\} + \alpha^2. \quad (19)$$

After some mathematical manipulations, the term $\mathbb{E}\left\{ \mu_{\rm a}(x) \mu_{\rm a}(-x) \right\}$ in (19) can be calculated as

$$\mathbb{E}\{\mu_{\rm a}(x) \mu_{\rm a}(-x)\} = 2\mathcal{C}_{\rm n} T_{\rm s}^2 e^{-\frac{(\psi_1 \kappa + 2\mathcal{C}_{\rm n}) \tau_{\rm d}}{N_{\rm a}}} \left(\psi_1 \kappa + \mathcal{C}_{\rm n} \right) Q\left(\kappa \right) + 2\mathcal{C}_{\rm n} T_{\rm s} e^{-\frac{\mathcal{C}_{\rm n} \tau_{\rm d}}{N_{\rm a}}} \mathcal{T}_3, \quad (20)$$

where $\mathcal{T}_3 = \int_0^{\kappa} \mu_{\rm a}(x) f_N(x) {\rm d}x$, which can be solved analytically as

$$\mathcal{T}_3 = \frac{T_{\rm s} \psi_1}{\sqrt{2\pi}} e^{-\frac{\mathcal{C}_{\rm n} \tau_{\rm d}}{N_{\rm a}}} \left[1 - e^{-\frac{1}{2}\kappa^2 - \frac{\psi_1 \tau_{\rm d} \kappa}{N_{\rm a}}} \right] + T_{\rm s} \left(\frac{\tau_{\rm d} \psi_1^2}{N_a} - \mathcal{C}_{\rm n} \right) e^{-\frac{\mathcal{C}_{\rm n} \tau_{\rm d}}{N_{\rm a}} + \frac{\psi_1^2 \tau_{\rm d}^2}{2 N_{\rm a}^2}} \left[Q\left(\kappa + \frac{\psi_1 \tau_{\rm d}}{N_{\rm a}} \right) - Q\left(\frac{\psi_1 \tau_{\rm d}}{N_{\rm a}} \right) \right]. \quad (21)$$

Finally, by substituting (20) and (19) into (16), the analytical expression of $\sigma^2_{W_{\rm d}}$ is achieved.

Since both noise terms in (11) are uncorrelated with the signal making it a standard additive Gaussian noise channel model, the SNR of the received signal is given by

$$\gamma = \frac{\alpha^2 \sigma_X^2}{\sigma^2_{W_{\rm d}} + \sigma^2_{W_{\rm s}}} = \frac{1}{\frac{1}{\gamma_{\rm d}} + \frac{1}{\gamma_{\rm s}}}. \quad (22)$$

where we denote the terms $\gamma_{\rm d} = 2\alpha^2 / \sigma^2_{W_{\rm d}}$ and $\gamma_{\rm s} = 2\alpha^2 / \sigma^2_{W_{\rm s}}$ the signal-to-distortion-noise ratio (SDNR) and signal-to-shot-noise ratio (SSNR), respectively. Note that α and $\sigma^2_{W_{\rm d}}$ are given by (9) and (16), respectively. The derivation of the analytical expression of the SNR is now complete. Equation (22) indicates that SNR depends on two factors, i.e., SDNR and SSNR. The BER of the considered system can be calculated by substituting γ into the QAM BER equation, e.g., [8, eq. (30)].

$$\sigma^2_{W_\mathrm{d}}[k] = \mathbb{E}\{|W_\mathrm{d}[k]|^2\} = \frac{1}{K}\sum_{n=0}^{K-1}\sum_{m=0}^{K-1}\mathbb{E}\{w_\mathrm{d}[n]w_\mathrm{d}[m]\}e^{-\frac{2\pi nkj}{K}+\frac{2\pi mkj}{K}}$$
$$= \frac{1}{K}\sum_{n=0}^{K-1}\mathbb{E}\{w_\mathrm{d}^2[n]\} + \frac{1}{K}\sum_{n=0}^{K-1}\mathbb{E}\{w_\mathrm{d}[n]w_\mathrm{d}[n_\mathrm{f}]\}e^{-\frac{2\pi nkj}{K}+\frac{2\pi n_\mathrm{f}kj}{K}} - \frac{1}{K}\sum_{n=0}^{K-1}\mathbb{E}^2\{w_\mathrm{d}[n]\}\,e^{-\frac{2\pi nkj}{K}}\sum_{m\neq n,n_\mathrm{f}}^{K-1}e^{\frac{2\pi mkj}{K}},$$
$$= \sigma^2_{w_\mathrm{d}} + \mathbb{E}^2\{w_\mathrm{d}[n]\} + \frac{\mathbb{E}\{w_\mathrm{d}[n]w_\mathrm{d}[n_\mathrm{f}]\}}{K}\underbrace{\sum_{n=0}^{K-1}e^{-\frac{2\pi nkj}{K}+\frac{2\pi n_\mathrm{f}kj}{K}}}_{\mathcal{T}_1} - \frac{\mathbb{E}^2\{w_\mathrm{d}[n]\}}{K}\underbrace{\sum_{n=0}^{K-1}e^{-\frac{2\pi nkj}{K}}\sum_{m\neq n,n_\mathrm{f}}^{K-1}e^{\frac{2\pi mkj}{K}}}_{\mathcal{T}_2}. \quad (12)$$

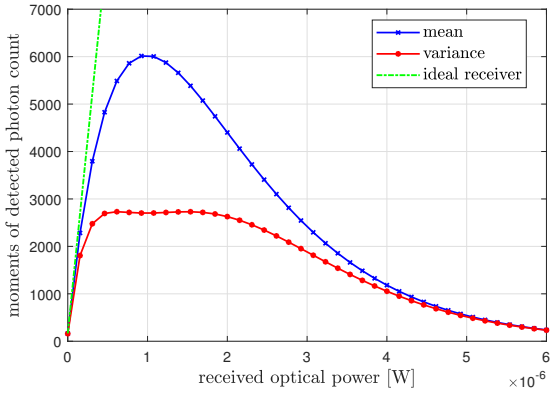

Fig. 1. The mean and variance of the detected photon count of the considered SPAD receiver versus the received optical signal power.

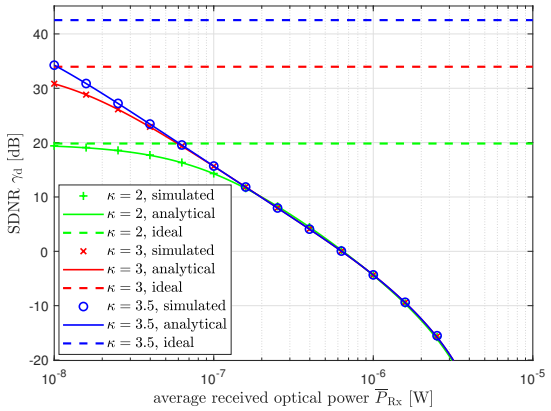

Fig. 2. The SDNR versus the received optical power with various clipping level.

IV. Numerical Results

In this section, the numerical performance analysis of the SPAD-based OFDM system is presented. Unless otherwise mentioned, the parameters used in the simulation are as follows: $K = 1024$, $T_\mathrm{s} = 20$ ns, $\Upsilon_\mathrm{PDE} = 0.35$, $N_\mathrm{a} = 8192$, $\tau_\mathrm{d} = 10$ ns, $P_\mathrm{B} = 10$ nW, $\vartheta_\mathrm{DCR} = 0.5$ MHz, $\varphi_\mathrm{AP} = 0.75\%$, $\varphi_\mathrm{CT} = 2.5\%$, $P_\mathrm{max} = 20$ mW, and the optical wavelength $\lambda_\mathrm{op} = 450$ nm [10], [11]. The average transmitted optical power $\overline{P}_\mathrm{Tx}$ can be calculated as described in Section II-A. By changing channel path loss ζ, various average optical power at the receiver $\overline{P}_\mathrm{Rx} = \zeta\,\overline{P}_\mathrm{Tx}$ can be achieved.

Fig. 1 presents the mean and variance of the SPAD receiver output versus the received optical power, which are calculated based on (4) and (5). It is shown that due to the existence of the dead time, the average detected photon count has nonlinear relationship with the received power. The variance of the photon count is signal dependent and is less than the mean value. This is different from the ideal photon counting receiver, i.e., when $\tau_\mathrm{d} = 0$, whose mean and variance of the detected photon count are identical and both increase linearly with the received optical power.

Fig. 2 shows the SDNR versus the received optical power with various clipping level. Note that for SPAD receiver, the considered nonlinear distortion contains both nonlinearities introduced by signal clipping at the transmitter and SPAD receiver as presented in (7). It is demonstrated that when the SPAD receiver is employed, with the increase of $\overline{P}_\mathrm{Rx}$, the SDNR decreases. This is because higher $\overline{P}_\mathrm{Rx}$ means wider utilized dynamic range of the receiver and hence severer receiver nonlinearity which leads to the lower SDNR. On the other hand, when the ideal photon counting receiver is used, the system is only influenced by signal clipping whose impacts do not change with $\overline{P}_\mathrm{Rx}$, resulting in the fixed SDNR over $\overline{P}_\mathrm{Rx}$. In addition, when $\overline{P}_\mathrm{Rx}$ is very small, the SDNR of the SPAD receiver converges to that of the ideal receiver due to the negligible SPAD nonlinearity. Fig. 2 further indicates that the system benefits from the higher κ, which can provide higher SDNR in low $\overline{P}_\mathrm{Rx}$ regime, because of the less nonlinearity induced by the signal clipping. However, when κ is beyond 3, since the nonlinear distortion caused by the signal clipping is sufficiently eliminated, the improvement introduced by high κ reduces. In high $\overline{P}_\mathrm{Rx}$ regime, since the SDNR turns to be limited by the SPAD nonlinearity whose impact is similar when various κ is employed, the same SDNR is achieved regardless of the value of κ. Fig. 3 presents the SSNR versus the received optical power. It is shown that different from the SDNR, the SSNR is not sensitive to the varying κ. For SPAD receiver, with the rise of $\overline{P}_\mathrm{Rx}$, SSNR initially increases but then drops because of the severer SPAD nonlinearity. This is distinct from the ideal linear detector whose SSNR monotonically increases with the rise of $\overline{P}_\mathrm{Rx}$. It is also worth noting that in Fig. 2 and Fig. 3 the analytical results of SDNR and SSNR perfectly match with the Monte Carlo simulation results. This validates our assumption of the effective additive Gaussian noise channel given in (11) which is derived based on CLT and Bussgang theorem.

The SNR of the considered SPAD-based OWC system with ACO-OFDM is given in (22), based on which the BER result can be achieved. Fig. 4 demonstrates the BER performance versus $\overline{P}_\mathrm{Rx}$ with $\kappa = 3$. Two modulation schemes, i.e.,

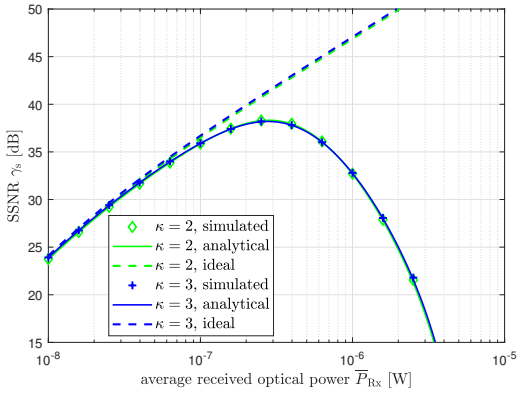

Fig. 3. The SSNR versus the received optical power.

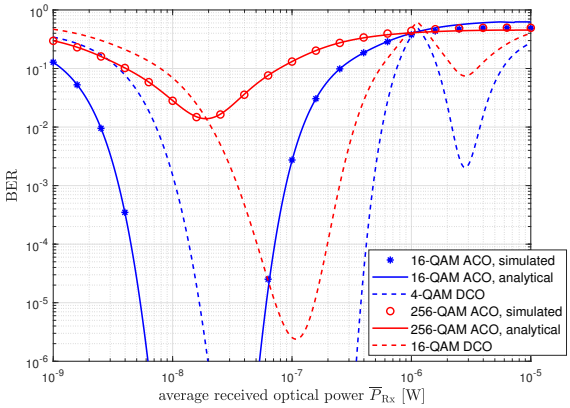

Fig. 4. The BER versus the received optical power for SPAD-based OWC system with OFDM.

16-QAM and 256-QAM are considered as examples. The theoretical and simulation results again confirm a close match which validates our analytical derivations. It is illustrated that with the increase of $\overline{P}_{\mathrm{Rx}}$, BER firstly drops and then increases. This is because in small $\overline{P}_{\mathrm{Rx}}$ regime, the system is limited by the shot noise, the initial increase of $\overline{P}_{\mathrm{Rx}}$ can effectively increase SSNR as shown in Fig. 3 and produce lower BER. However, in high $\overline{P}_{\mathrm{Rx}}$ regime, the gain of SSNR is overtaken by the SPAD nonlinear distortion. As presented in Fig. 2, higher $\overline{P}_{\mathrm{Rx}}$ brings less SDNR, which results in higher BER. In addition, employing larger modulation order, e.g., 256-QAM, introduces worse BER performance, as expected. Besides the system with ACO-OFDM, the performance of the system with DCO-OFDM is also considered for comparison. The detailed performance analysis of SPAD-based OWC system with DCO-OFDM is presented in [5]. Because the spectral efficiency of the ACO-OFDM is half of the DCO-OFDM, to make a fair comparison between the schemes, the M-QAM ACO-OFDM should be compared with $\sqrt{M}$-QAM DCO-OFDM. It is illustrated that in the lower $\overline{P}_{\mathrm{Rx}}$ regime, 16-QAM ACO-OFDM is more power efficient and requires around 4 dB less optical power than 4-QAM DCO-OFDM to achieve the same BER. However, in the high power regime, the latter in turn outperforms the former. For example, with a target BER of 10^{-3}, the received optical power should be less than 0.09 μW when 16-QAM ACO-OFDM is employed. However, this maximal tolerable power extends to 0.5 μW when 4-QAM DCO-OFDM is employed, which is 7.4 dB higher against its ACO counterpart. This is because for the same $\overline{P}_{\mathrm{Rx}}$, ACO-OFDM signal spans over wider dynamic range compared to DCO-OFDM signal and thus experiences stronger receiver nonlinear distortion, which degrades its performance in high power scenarios. Note that for DCO-OFDM the extra dip of BER in high optical power scenario was explained in [5]. In addition, the comparison between 256-QAM ACO-OFDM and 16-QAM DCO-OFDM indicates that the superiority of ACO-OFDM in the low power regime drops when larger constellations are employed. Therefore, in the practical implementation, the employed OFDM schemes should be designed by considering both the received optical power and spectral efficiency requirement.

V. Conclusion

ACO-OFDM can be used in SPAD-based OWC systems to achieve a good compromise between the high spectral efficiency and energy efficiency. In this work, a theoretical performance analysis of SPAD-based OWC systems with ACO-OFDM is presented. The analytical expressions of SNR and BER are derived which match with the Monte Carlo simulation results perfectly. Through extensive numerical results, the impact of the SPAD nonlinearity on the system performance is investigated. It is further demonstrated that in the lower power regimes, ACO-OFDM is superior to DCO-OFDM (e.g., 4 dB power gain achieved by 16-QAM ACO-OFDM over 4-QAM DCO-OFDM); whereas, in the high power regimes DCO-OFDM is more preferable.

References

[1] S. Huang and M. Safari, "SPAD-based optical wireless communication with signal pre-distortion and noise normalization," *IEEE Trans. Commun.*, vol. 70, no. 4, pp. 2593–2605, 2022.

[2] W. Matthews *et al.*, "A 3.45 Gigabits/s SiPM-based OOK VLC receiver," *IEEE Photon. Technol. Lett.*, vol. 33, no. 10, pp. 487–490, 2021.

[3] S. Huang *et al.*, "5 Gbps optical wireless communication using commercial SPAD array receivers," *Opt. Lett.*, vol. 47, no. 9, pp. 2294–2297, May 2022.

[4] L. Zhang *et al.*, "A simplified post equalizer for mitigating the nonlinear distortion in SiPM based OFDM-VLC system," *IEEE Photonics Journal*, vol. 14, no. 1, pp. 1–7, 2022.

[5] S. Huang *et al.*, "Performance analysis of SPAD-based optical wireless communication with OFDM," *J. Opt. Commun. Netw.*, vol. 15, no. 3, pp. 174–186, Mar 2023.

[6] J. Armstrong and B. J. Schmidt, "Comparison of asymmetrically clipped optical OFDM and DC-biased optical OFDM in AWGN," *IEEE Communications Letters*, vol. 12, no. 5, pp. 343–345, 2008.

[7] D. Tsonev, S. Sinanovic, and H. Haas, "Complete modeling of nonlinear distortion in OFDM-based optical wireless communication," *Journal of Lightwave Technology*, vol. 31, no. 18, pp. 3064–3076, 2013.

[8] S. Dimitrov, S. Sinanovic, and H. Haas, "Clipping noise in OFDM-based optical wireless communication systems," *IEEE Transactions on Communications*, vol. 60, no. 4, pp. 1072–1081, 2012.

[9] M. J. Hasan *et al.*, "An energy-efficient optical wireless OFDMA scheme for medical body-area networks," *IEEE Transactions on Green Communications and Networking*, vol. 6, no. 3, pp. 1806–1818, 2022.

[10] ON Semiconductor, "J-SERIES SIPM: Silicon photomultiplier sensors, J-Series (SiPM)," Accessed: Mar 9, 2023. [Online]. Available: https://www.onsemi.com/products/sensors/silicon-photomultipliers-sipm/j-series-sipm.

[11] S. M. Patanwala *et al.*, "A high-throughput photon processing technique for range extension of SPAD-based lidar receivers," *IEEE Open Journal of the Solid-State Circuits Society*, vol. 2, pp. 12–25, 2022.